

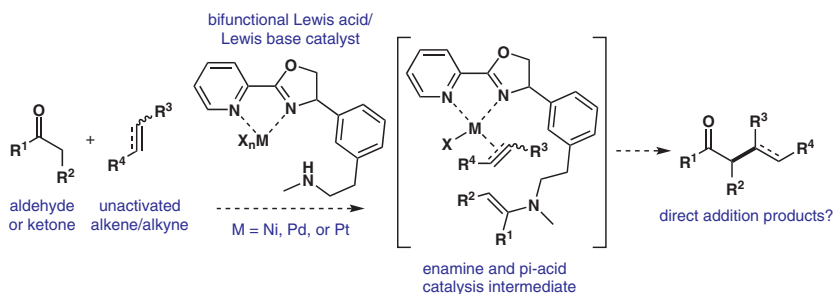
DFT-Assisted Design and Evaluation of Bifunctional Amine/Pyridine-Oxazoline Metal Catalysts for Additions of Ketones to Unactivated Alkenes and Alkynes

Eric Greve

Jacob D. Porter

Chris Dockendorff* 

Department of Chemistry, Marquette University,
P. O. Box 1881, Milwaukee, WI 53201-1881, USA
christopher.dockendorff@mu.edu



Received: 19.07.2018

Accepted: 28.08.2018

Published online: 02.10.2018

DOI: 10.1055/s-0037-1610285; Art ID: ss-2018-m0483-op

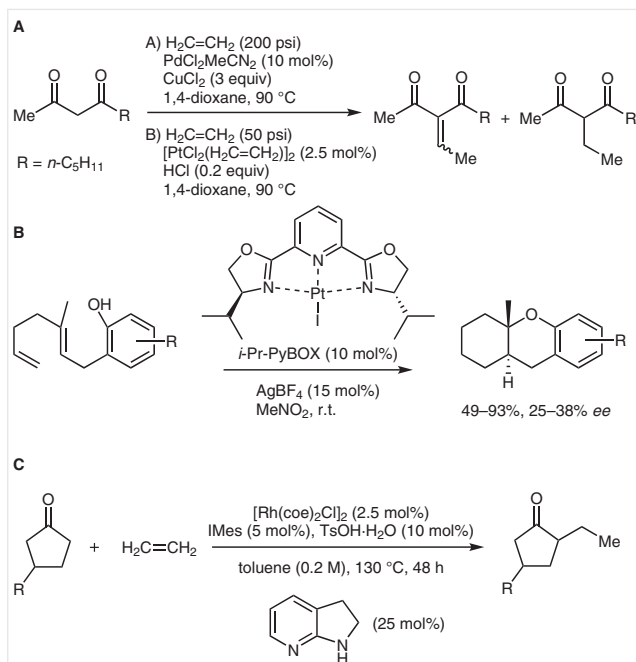
Abstract Bifunctional catalyst systems for the direct addition of ketones to unactivated alkenes/alkynes were designed and modeled by density functional theory (DFT). The designed catalysts possess bidentate ligands suitable for binding of pi-acidic group 10 metals capable of activating alkenes/alkynes, and a tethered organocatalyst amine to activate the ketone via formation of a nucleophilic enamine intermediate. The structures of the designed catalysts before and after C–C bond formation were optimized using DFT, and reaction steps involving group 10 metals were predicted to be significantly exergonic. A novel oxazoline precatalyst with a tethered amine separated by a meta-substituted benzene spacer was synthesized via a 10-step sequence that includes a key regioselective epoxide ring-opening step. It was combined with group 10 metal salts, including cationic Pd(II) and Pt(II), and screened for the direct addition of ketones to several alkenes and an internal alkyne. ^1H NMR studies suggest that catalyst-catalyst interactions with this system via amine–metal coordination may preclude the desired addition reactions. The catalyst design approach disclosed here, and the promising calculations obtained with square planar group 10 metals, light a path for the discovery of novel bifunctional catalysts for C–C bond formation.

Key words alkylation, alkene complexes, platinum, bifunctional catalysis, organocatalysis, ketones, DFT, catalyst design

The forging of carbon–carbon bonds via transition-metal-catalyzed additions to activated alkenes and alkynes has been a popular synthetic strategy in recent decades. Of particular utility have been the addition of diverse organometallic nucleophiles to α,β -unsaturated compounds using rhodium, palladium, and copper catalysts, as well as additions to allylic electrophiles (e.g., Tsuji–Trost-type reactions). Catalytic C–C bond formations involving additions to unactivated alkenes are less common, and comprise examples such as Heck reactions¹ and Zr-catalyzed asymmetric carboalumination of alkenes (ZACA reaction).² The catalytic direct addition of aldehydes/ketones to unactivated alkenes

and alkynes is a desirable complementary transformation that could be a general strategy for the α -functionalization of carbonyl compounds, and has the additional advantage of perfect atom economy. Examples of such reactions in an intramolecular fashion (Conia-ene type reaction) have been reported,^{3–11} but intermolecular examples are very rare. Three innovative examples of alkene hydroalkylation reactions are given in Scheme 1. Widenhoefer reported Pd(II)- and Pt(II)-catalyzed additions of stabilized nucleophiles (from 1,3-diones) to ethylene and propylene, where the metal is presumed to act as a pi-Lewis acid for alkene activation (Scheme 1, A).¹² Vitagliano reported a similar hydroalkylation reaction using 2,6-bis(diphenylphosphinomethyl)pyridine (PNP) Pd(II) and Pt(II) complexes.¹³ A related approach has been utilized by Gagné and co-workers for the intramolecular cyclization of phenolic dienes using a PyBOX-Pt(II) complex (Scheme 1, B).^{14,15} Dong has reported a dual rhodium and amine catalyst system (thought to act as a single molecule, bifunctional catalyst¹⁶) for the direct addition of ketones to alkenes (Scheme 1, C)¹⁷ and alkynes.¹⁸ Despite these significant advances, more general, active, and less-sensitive catalysts, especially those that may facilitate asymmetric reactions, would be of great benefit.

In the challenge to discover novel addition reactions with unactivated alkenes and alkynes, we were inspired by both intramolecular (Conia-ene) reactions, and intermolecular Wacker-type reactions with heteroatom nucleophiles,^{19–21} particularly since these reactions can be reasonably functional group-tolerant and can in some cases be run under aqueous conditions. The utility of amine catalysts for the activation of aldehyde/ketone pronucleophiles (enamine catalysis) is well-established,²² however, our recent work has confirmed that π -acidic metal catalysts typically used to activate alkenes and alkynes²³ may not be compatible with enamine intermediates, which may out-



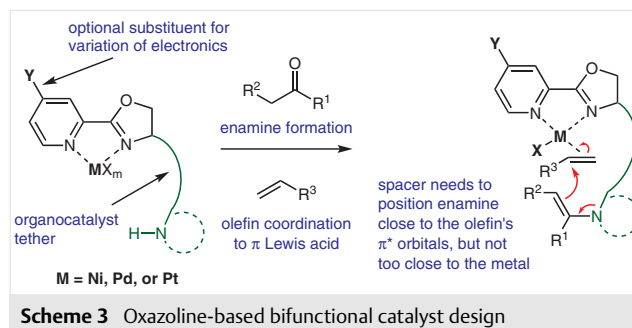
Scheme 1 Prior examples of catalytic direct additions to alkenes

compete the alkene/alkyne substrate as ligands for the metal.²⁴ We reasoned that bifunctional catalysts¹⁶ with carefully positioned organocatalytic (amine) and π -acidic sites may avoid self-quenching and facilitate ‘pseudo-intramolecular’ reactions between separate aldehydes/ketones and alkenes/alkynes (Scheme 2). Our first investigation into this strategy focused on distorted tetrahedral Cu(I) systems;²⁴ herein are disclosed our first efforts to develop bifunctional catalysts based on square planar group 10 metal complexes [nickel(II), palladium(II), and platinum(II)].

Design of Bifunctional Catalysts and Prioritization with Density Functional Theory (DFT) Calculations

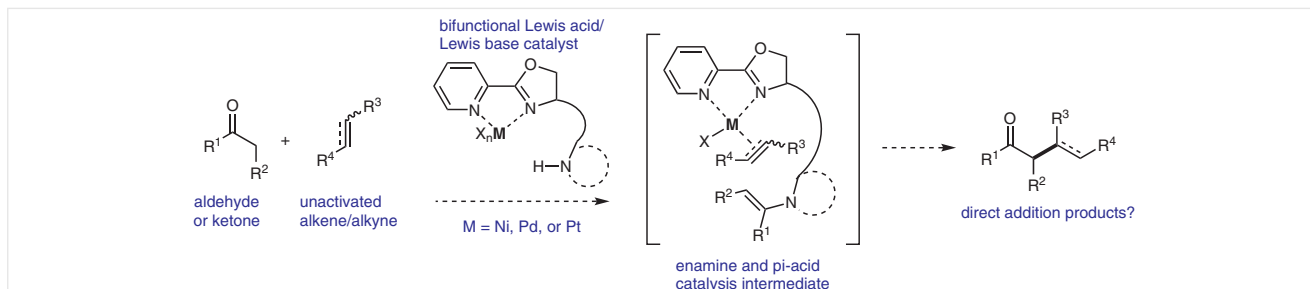
A key challenge to the development of effective bifunctional catalysts for activation of nucleophilic and electrophilic partners is the requirement that the catalytic centers

are close enough to facilitate the desired bond formation, but not so close that self-quenching occurs. In this manner, the bifunctional catalysts under study here are conceptually related to the use of frustrated Lewis pairs (FLPs).²⁵ We investigated several novel ‘carrot-and-stick’-like designs with rigid spacers that could reliably separate the Lewis acidic and basic centers (Scheme 2). *Meta*-substituted aromatic groups have proven to be effective building blocks for this purpose, which we have combined with several oxazoline-containing ligands that have demonstrated utility with group 10 metals. We reasoned that harder nitrogen-based ligands, such as those utilized in Wacker-type reactions, could be effective at stabilizing cationic metals suitable for activating alkenes and alkynes for outer sphere attack of enamine nucleophiles. A representative example of our catalyst design is depicted in Scheme 3.

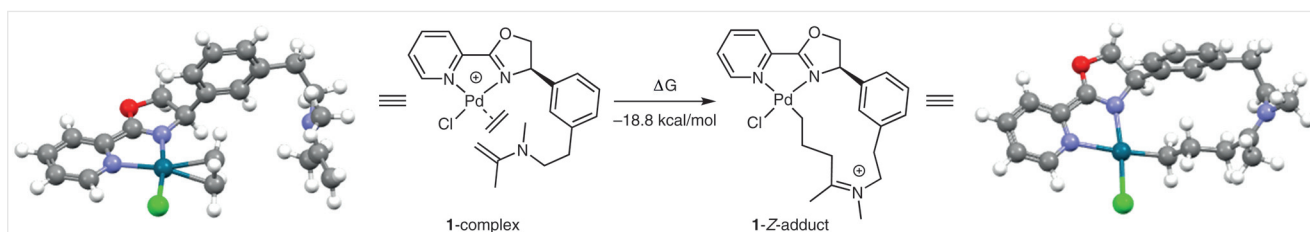


Scheme 3 Oxazoline-based bifunctional catalyst design

A significant disadvantage to the use of bifunctional catalysts is the increased complexity and lack of tunability relative to dual (cooperative) catalysts. This challenge (and bottleneck) of bifunctional catalyst synthesis motivated us to explore computational approaches for the prioritization of new catalyst designs. Using our recently disclosed approach using density functional theory (DFT) calculations,²⁴ we optimized bifunctional catalyst structures before and after C–C bond formation, and calculated the associated free energy changes. We assume that for catalysis to be feasible, this step needs to be exergonic, and the calculated free energy changes can be used as a reasonably rapid tool to prioritize catalyst designs. We anticipate using transition state energy calculations for more comprehensive modeling



Scheme 2 Our strategy for the catalysis of direct additions of aldehydes/ketones to alkenes/alkynes



Scheme 4 Representative computed example of putative intermediate enamine-PyOX-metal-alkene complex (left), and iminium adduct after C–C bond formation (right)

of catalytic cycles with operational catalysts in the future. We used the LANL2DZ²⁶ basis set for transition metals, and cc-pVDZ²⁷ for all other atoms.

Inspired by Gagné and co-workers' use of Pt(II)-PyBOX complexes for the catalytic cyclization of a variety of phenolic polyenes to generate polycyclic structures,^{14,15} we focused on a pyridine-oxazoline moiety in our initial bifunctional catalyst design. Our bifunctional catalysts require a π -Lewis acid chelating ligand with a pendant organocatalyst. The organocatalyst tether needs to position the activated aldehyde/ketone (i.e., enamine intermediate) close to the π^* -orbital of a complexed olefin, to facilitate the desired C–C bond formation (Scheme 3). We reasoned that the square planar coordination geometries of Group 10 metal complexes could satisfy this stereoelectronic requirement while preventing amine/enamine-metal self-poisoning. Our initial goal was to determine suitable ligand and organocatalyst tether combinations capable of promoting nucleophilic addition to alkenes. We examined the attachment point of the tether, the tether length, and the use of different 1° and 2° amines as the organocatalytic component.

One logical tether placement is at the 4-position of the oxazoline. An aryl substituent was found to minimize steric interactions between the coordinated olefin and the tether, and positions the organocatalyst an appropriate distance from the metal center. Additionally, the aryl substituent provides rigidity to the tether which may prevent self-quenching. After using physical models to examine hypothetical transition states for the C–C bond forming step and ensuring a favorable geometry of the enamine with respect to the π^* -orbitals of the coordinated olefins, the most promising scaffold **1** was optimized using DFT (Scheme 4).

Optimization of complex geometries and calculation of energies via DFT of the Pt(II)-ethylene complex (**1-complex**) and the iminium adduct after C–C bond formation (**1-Z-adduct**) indicated that the free energy change is favorable for this catalytic step in the direct addition of acetone to ethylene (Table 1; complete calculations with both Pd and Pt are in Table S1). The DFT calculations reported in Tables 1 and 2 are for the *Z*-iminium adducts, which were found to be more stable than the *E*-iminium adducts. We sought to test the effect of the tether length and position of substitution on the aryl ring in precatalyst **1** (Table 1). The catalyst with the tether attached to the *meta*-position of the arene was the most favorable, confirming our hypothesis using

Table 1 DFT Calculations for C–C Bond Formation with Variable Tether Lengths and Positions^a

Entry	Amine tether location	<i>n</i>	Quenched ΔG^1 (kcal/mol)	Adduct ΔG^2 (kcal/mol)
1	<i>ortho</i>	1	–18.5	–14.9
2	<i>meta</i>	1	–7.2	–17.5
3	<i>para</i>	1	–0.2	–13.1
4	<i>meta</i>	0	4.0	–6.7
5	<i>meta</i>	2	–15.3	–19.0

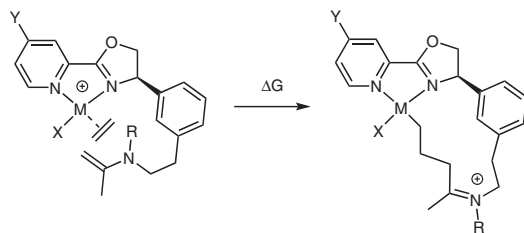
^a All calculations used functional B3PW91, basis set LANL2DZ for metals, and basis set cc-pVDZ for all other atoms, using dichloromethane as solvent.

3D models. Positioning the tether at the *ortho*-position (Table 1, entry 1, $\Delta G^2 = -14.9$ kcal/mol) seems reasonable given its comparable thermodynamics to the *meta*-position (entry 2, $\Delta G^2 = -17.5$ kcal/mol), however, this would place the amine or enamine in closer proximity to poison the metal. This phenomenon was observed when performing DFT optimization on the enamine adding to the Pt(II) center and displacing ethylene to give the 'quenched' structures (Table 1; complete data for both Pt and Pd are in Table S2). When the tether is in the *ortho*-position, the addition of the enamine to the metal is calculated to be more favorable than the desired addition to ethylene (entry 1, $\Delta G^1 = -18.5$ kcal/mol vs $\Delta G^2 = -14.9$ kcal/mol). Moving the tether to the *meta*- or *para*-position (entries 2, 3) results in the desired adduct formation to be at least 10 kcal/mol more favorable than intramolecular quenching. As the length of the alkyl chain increases, the C–C bond formation is calculated to become more exergonic. A tethered ethylamine (entry 2) was found to be ideal. A shorter chain length (entry 4, $\Delta G^2 = -6.7$ kcal/mol) is less exergonic, and a catalyst with a longer chain length (entry 5, $\Delta G^2 = -19.0$ kcal/mol) is calculated to be most favorable for this transformation, but will likely lead to self-quenching via amine–metal coordination (DFT calculations in Table S2). Overall, these preliminary DFT calculations led us to prioritize the catalyst of entry 2 (Table 1) as our lead scaffold to study in further detail.

We sought to study the effect of the metal counter ion X and the electronics of the pyridyl ring (substituent Y) on the C–C bond forming step (Table 2). More weakly coordinating counterions result in more exergonic calculated reactions (Table 2, entries 1–4), though it should be emphasized that solvent effects, particularly with the cationic metals under study here, may be difficult to quantify using these calculations. The weaker sigma donors yield more electrophilic metal centers, which in turn are expected to generate a more electrophilic ethylene complex that should provide more exergonic reactions. Although not as prominent, this trend was also observed for 4-substituted pyridyl precatalysts. Electron-withdrawing substituents (entries 7, 8) yielded a more exergonic C–C bond formation, and the electron-donating methoxy group (entry 9) resulted in a less exergonic reaction, though fluoride (entry 6, $\Delta G = -17.2$ kcal/mol) was calculated to be equivalent to hydrogen (entry 5) with the use of a cationic palladium catalyst.

These ligands were designed to provide square planar coordination geometries with group 10 transition metals. A square planar coordination geometry allows the coordinated alkene to be 'sandwiched' between the metal and the appended enamine intermediate, providing access to the π^* -orbitals on the alkene. Coordination of an alkene in this fashion, *cis* to the oxazoline and proximal to the organocatalyst tether, was found to be 3.0 kcal/mol more favorable than the *trans* coordination (Supporting Information, Figure S1). When using a group 11 metal, such as Cu(I) (Table

Table 2 DFT Calculations for C–C Bond Formation Examining the Metal Counterion and Ligand Electronics^a



Entry	X	Y	R	M	ΔG (kcal/mol)
1	Cl	H	Me	Pd	-18.8
2	Br	H	Me	Pd	-19.9
3	I	H	Me	Pd	-20.5
4	PF ₆	H	Me	Pd	-30.8
5	Cl	H	H	Pd	-17.2
6	Cl	F	H	Pd	-17.2
7	Cl	Cl	H	Pd	-18.5
8	Cl	Br	H	Pd	-19.0
9	Cl	OMe	H	Pd	-15.0
10	Cl	H	Me	Ni	-16.8
11	Cl	H	Me	Pt	-17.5
12	Cl	H	Me	Cu(I)	+28.5

^a All calculations used functional B3PW91, basis set LANL2DZ for metals, and basis set cc-pVDZ for all other atoms, using dichloromethane as solvent.

2, entry 12), the ethylene complex takes on a distorted tetrahedral coordination geometry, thus positioning the alkene π^* -orbitals much further away from the enamine (Supporting Information, Figure S2). The macrocyclization for Cu(I) with the precatalyst of entry 12 (Table 2) is calculated to be very endergonic, in contrast to the group 10 metals (entries 1, 10, 11), confirming the importance of a square planar geometry with our designed precatalyst. It is notable that the C–C bond formation steps with the group 10 metal complexes in Tables 1 and 2 are calculated to be significantly more exergonic than the corresponding reaction steps with our prior Cu(I) complexes designed to catalyze additions to unactivated alkenes.²⁴

While these ground state DFT calculations are used to screen our precatalysts for exergonicity of the C–C bond forming step, the activation energy for this step also determines the catalyst viability. Given the computationally intensive nature of calculating these transition states, we sought to estimate the activation energy by fixing the distance between the new C–C bond formed between the ethylene carbon (C1) and enamine (C2), optimizing the geometries of the molecule, and calculating the resulting energies (Figure 1; calculations in Table S3). The free energies reported are with respect to the lowest energy conformation

of the ethylene complex (Supporting Information, Figure S3). The free energy barrier for the C–C bond formation was found to be 7.4 kcal/mol, with 4.1 kcal/mol of that energy arising from the organocatalyst tether changing from an extended conformation (C1–C2 = 9.035 Å) to a more closed conformation (C1–C2 = 5.065 Å). This energy barrier should be low enough to overcome at elevated temperatures.

Synthesis of Precatalyst

Based on our DFT calculations, we pursued the synthesis of the bifunctional precatalyst **1** (Scheme 5). Our initial efforts aimed at a late stage *N*-alkylation of the organocatalyst moiety in an effort to develop a modular synthesis for the preparation of different secondary amines. However, our early attempts at amine alkylation, lead to over alkylation (not shown). We instead chose to implement an *N*-methylation earlier in the synthesis. First, 3-bromobenzeneacetonitrile was reduced using in situ formed alane (AlH_3),²⁸ using a protocol reported by Leung and co-workers.²⁹ The resulting amine **3** was Boc-protected (yielding **4**), then *N*-methylated using potassium hydroxide and iodomethane to afford **5** in good yield. Suzuki coupling of aryl bromide **5** with potassium vinyltrifluoroborate³⁰ generated the substituted styrene **6**, with more consistent results

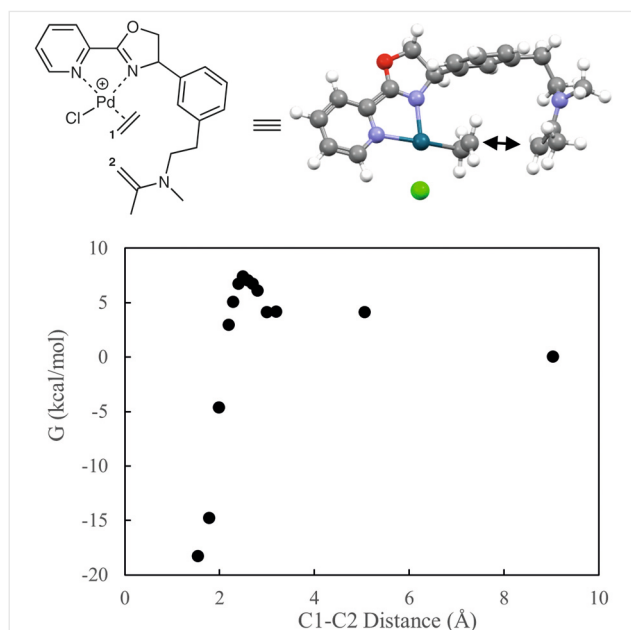
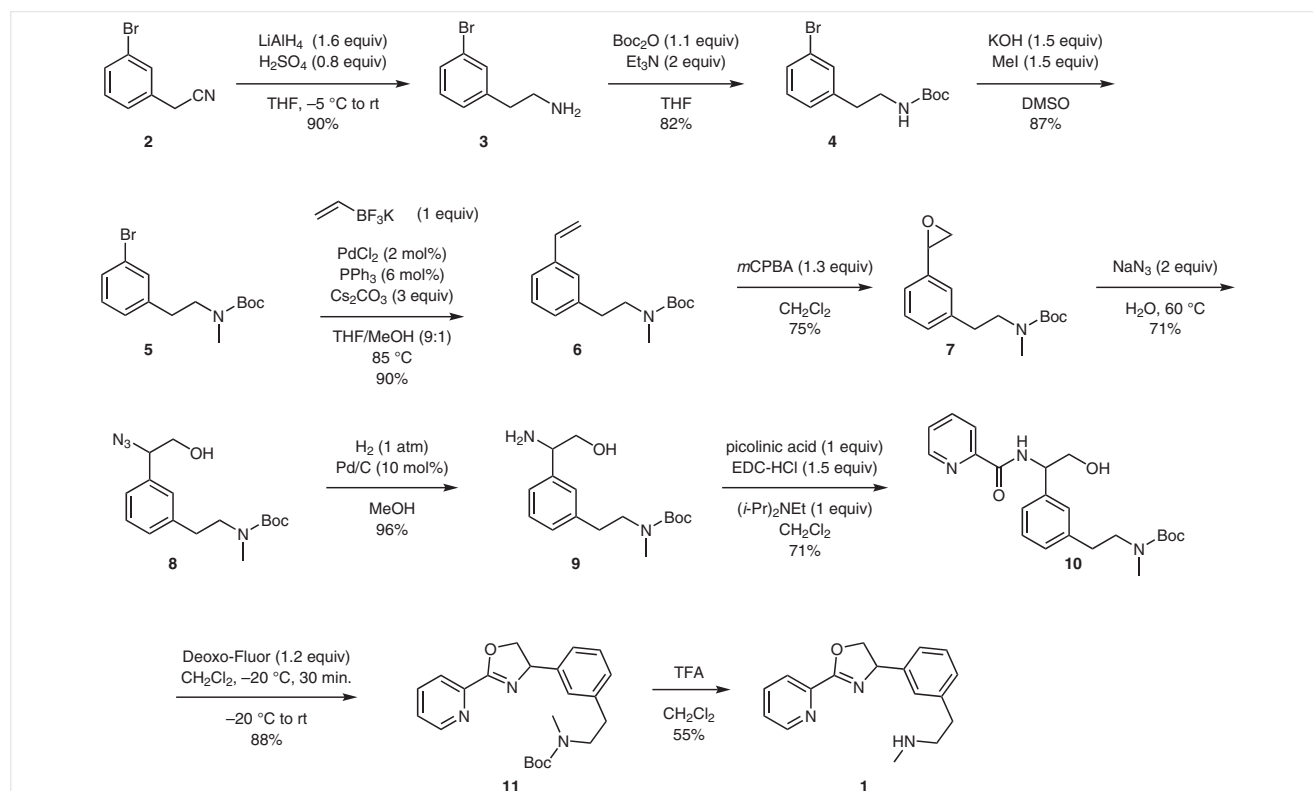


Figure 1 Estimation of transition state energy for C–C bond formation by DFT calculations of structures with fixed distances between enamine and ethylene. Values are normalized to the complex in its most stable conformation prior to C–C bond formation (which is set to $G = 0$ kcal/mol).



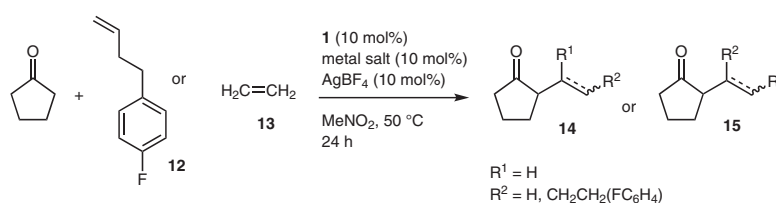
Scheme 5 Synthesis of bifunctional PyOX precatalyst

compared to vinyl triboroxine–pyridine complex. Subsequent epoxidation of styrene **6** with *m*CPBA followed by regioselective ring-opening with sodium azide in hot water yielded the azide **8** in 66% yield over the two steps. While this synthetic route yields racemic material, optically active catalysts could be generated via asymmetric epoxidation methods. The current styrene epoxide opening method using sodium azide and hot water has been shown to give clean inversion of stereochemistry.³¹ Reduction of **8** using Pd/C under H₂ afforded amino alcohol **9** in excellent yield. EDC peptide coupling with picolinic acid followed by oxazoline formation using Deoxo-Fluor[®]^{32,33} proceeded smoothly to afford **11**. Finally, Boc removal using excess trifluoroacetic acid (TFA) yielded the final precatalyst **1**. Current efforts are focused on a late stage reductive amination reaction to introduce organocatalytic amines.

Reaction Screening

With the synthesized precatalyst **1** in hand, we proceeded to test it in a variety of reaction screens for the direct additions of ketones to alkenes and alkynes, using GC-MS to analyze each reaction. Cyclopentanone was selected due to its well-established reactivity for enamine formation.³⁴ Additionally, methyl acetoacetate was chosen for its frequent use in alkene hydroalkylation reactions. Ethylene (**13**), 4-(4-fluorophenyl)-1-butene (**12**), and 6-phenyl-2-hexyne (**16**) were chosen as electrophiles in the reactions; the aromatic handles were included with several substrates to facilitate product identification. Due to its polar, non-coordinating nature, nitromethane was used for all reactions; less polar solvents are often unable to dissolve the cationic metal salts of interest. For metal salts with halide counterions, the metal/precatalyst solution was reacted with **1** or **2**

Table 3 Screening of Group 10 Metal Salts in Reactions with Cyclopentanone



Entry ^{a,b}	Metal	Result with: ^c	
		12	13 ^b
1	NiCl ₂ ·6H ₂ O/ AgBF ₄	A	A
2	NiI ₂ /AgBF ₄	A	A
3	Ni(OAc) ₂ ·4H ₂ O	A	A
4	NiCl ₂ (DME)/AgBF ₄	A	A
5	Ni(OTf) ₂	A	A
6	Pd(OAc) ₂	A	A
7	Pd(MeCN) ₄ (BF ₄) ₂	B	A
8	Pd(MeCN) ₂ Cl ₂ /AgBF ₄	B	A
9	Pt(DMSO) ₂ Cl ₂ /AgBF ₄	A	A
10	Pt(DMSO) ₂ I ₂ /AgBF ₄	A	A
11	Pt(DMSO) ₂ Cl ₂ /2AgBF ₄	A	A
12	Pt(DMSO) ₂ I ₂ /2AgBF ₄	A	A
13	AgBF ₄	A	A
14	none	A	A
15	Pd(MeCN) ₄ (BF ₄) ₂ ^d	C	C
16	Pd(MeCN) ₂ Cl ₂ /AgBF ₄ ^d	C	C

^a Precatalyst **1** (2 mg, 0.007 mmol) was dissolved in MeNO₂ (0.3 mL) and added to the respective metal salt (0.007 mmol) in a 1.5 mL HPLC vial. The alkene (0.070 mmol) and cyclopentanone (0.070 mmol) were added as solutions in MeNO₂ (0.100 mL). The vials were heated at 50 °C for 24 h, and analyzed directly via GC-MS.

^b Reactions were flushed with ethylene and stirred at 50 °C for 24 h at 50 psi in a pressure flask.

^c Results: A: No reaction; B: Trace amount of alkene dimerization; C: Alkene oligomerization observed.

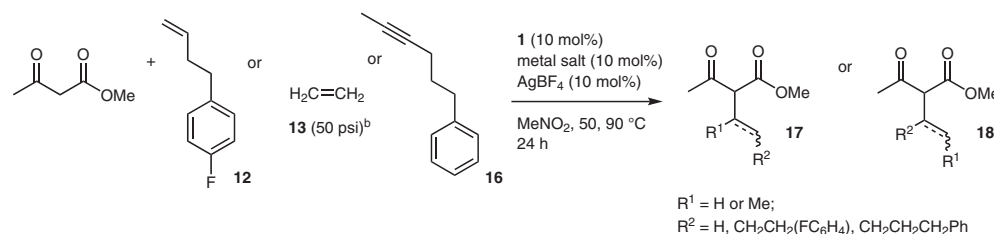
^d No precatalyst was used.

equivalents of silver tetrafluoroborate, and the resulting silver halide salts were filtered off prior to the addition of substrates.

Results from a representative metal salt screen with precatalyst **1**, cyclopentanone, and either ethylene (**13**) or 4-(4-fluorophenyl)-1-butene (**12**) are given in Table 3. All reactions with ethylene (Table 3, entries 1–16) produced no detectable desired products such as **14** or **15** via GC-MS, as confirmed by analysis of low concentrations of the positive control 2-ethylcyclopentanone (**14a**, R¹, R² = H) added to a sample reaction mixture. Similarly, when 4-(4-fluorophenyl)-1-butene (**12**) was used (entries 1–16), no desired adducts were detected and only starting material peaks were

prominent in the GC-MS traces. Olefin isomerization products and trace amounts of dimerization products were found in samples with **12** and palladium metals (entries 7, 8). Precatalyst **1** appears to suppress olefin oligomerization, as control reactions without **1** (entries 15, 16) had nearly complete consumption of **12** and conversion to alkene dimer and trimers, as detected by GC-MS. In the case of ethylene, a peak with a mass corresponding to octene was detected in the GC-MS. Pt(II) and Pd(II) salts are known to promote the polymerization of alkenes.^{35–37} A reaction screen for the addition of cyclopentanone to 6-phenyl-2-hexyne was also performed, but also yielded only peaks for the starting materials in the GC-MS.

Table 4 Screening of Group 10 Metal Salts in Reactions with Methyl Acetoacetate



Entry ^{a,b}	Metal	Result with: ^c		
		12	13^b	16
1	NiCl ₂ (DME)/AgBF ₄	A	A	A
2	Ni(OTf) ₂	A	A	A
3	Pd(MeCN) ₄ (BF ₄) ₂	B	A	A
4	Pd(MeCN) ₂ Cl ₂ /AgBF ₄	B	A	A
5	Pt(DMSO) ₂ Cl ₂ /AgBF ₄	A	A	A
6	Pt(DMSO) ₂ I ₂ /AgBF ₄	A	A	A
7	Pt(DMSO) ₂ Cl ₂ /2AgBF ₄	A	A	A
8	Pt(DMSO) ₂ I ₂ /2AgBF ₄	A	A	A
9	AgBF ₄	A	A	A
10	–	A	A	A
11 ^d	Pt(DMSO) ₂ Cl ₂ /AgBF ₄	–	C	A
12 ^d	Pt(DMSO) ₂ I ₂ /AgBF ₄	–	C	A
13 ^d	Pt(DMSO) ₂ Cl ₂ /2AgBF ₄	–	C	A
14 ^d	Pt(DMSO) ₂ I ₂ /2AgBF ₄	–	C	A
15 ^{d,e}	Pt(DMSO) ₂ Cl ₂ /AgBF ₄	–	C	D
16 ^{d,e}	Pt(DMSO) ₂ I ₂ /AgBF ₄	–	C	D
17 ^{d,e}	Pt(DMSO) ₂ Cl ₂ /2AgBF ₄	–	C	D
18 ^{d,e}	Pt(DMSO) ₂ I ₂ /2AgBF ₄	–	C	D

^a Precatalyst **1** (2 mg, 0.007 mmol) was dissolved in MeNO₂ (0.3 mL) and added to the respective metal salt (0.007 mmol) in a 1.5 mL HPLC vial. The alkene or alkyne (0.070 mmol) and methyl acetoacetate (0.070 mmol) were added as solutions in MeNO₂ (0.100 mL). The vials were heated at 50 °C for 24 h, and analyzed directly via GC-MS.

^b Reactions were flushed with ethylene and stirred at 50 °C for 24 h at 50 psi in a pressure flask.

^c Results: A: No reaction; B: Trace amount of olefin dimerization; C: A peak with a mass corresponding to octene was present in the GC-MS; D: Alkyne dimerization and trimerization observed.

^d Reaction vials were heated at 90 °C for 24 h.

^e Precatalyst **1** was not added to these reaction vials.

Due to the limited solubility of some of the nickel metal salts and $\text{Pd}(\text{OAc})_2$ with our precatalyst in MeNO_2 , we chose to exclude these metal salts in our additional screens. Mixtures of methyl acetoacetate with ethylene (**13**), 4-(4-fluorophenyl)-1-butene (**12**), or 6-phenyl-2-hexyne (**16**) were screened with precatalyst **1** and either palladium or platinum metal salts (Table 4). Similar results were obtained as in the screens using cyclopentanone. Only starting material peaks were present in the GC-MS, except when using palladium with 4-(4-fluorophenyl)-1-butene, where trace amounts of isomerized alkene and dimerization products were detected. Due to the observed lack of reactivity, platinum monocationic and biscationic metal salt systems were tested at 90 °C for the addition of methyl acetoacetate to either ethylene or 6-phenyl-2-hexyne (**16**). In the absence of precatalyst **1**, ethylene presumably underwent oligomerization, as a peak with a mass corresponding to octene was detected by GC-MS (entries 15–18). Additionally, 6-phenyl-2-hexyne in the absence of **1** underwent dimerization and trimerization. With the incorporation of precatalyst **1**, the alkyne dimers and trimers were completely suppressed when using 6-phenyl-2-hexyne, but a detectable amount of octene was present when using ethylene.

A range of acid additives was additionally tested for the addition of methyl acetoacetate to ethylene, along with the non-coordinating base 2,6-di-*tert*-butylpyridine (Table 5). These reactions were initially run at 50 °C for 24 hours, and allowed to cool to room temperature before ~50 μL aliquots were taken for GC-MS analysis, then the temperature was increased to 90 °C for an additional 24 hours. No reactions were observed with any of the additives after heating at 50 or 90 °C.

Table 5 Additive Screen

Entry ^a	Additive	Result ^b
1	4-nitrophenol	NR
2	benzoic acid	NR
3	<i>p</i> -TsOH	NR
4	AcOH	NR
5	TFA	NR
6	2,6-di- <i>tert</i> -butylpyridine	NR
7	–	NR

^a Precatalyst **1** (1 mg, 0.0035 mmol) and $\text{Pd}(\text{MeCN})_4(\text{BF}_4)_2$ (0.0035 mmol) were dissolved in MeNO_2 (0.05 mL) in a 1.0 mL test tube. Methyl acetoacetate (0.035 mmol) and the additive (0.0035 mmol) were added as solutions in MeNO_2 (0.100 mL). The samples were heated at 50 °C for 24 h, aliquots were taken for analysis directly via GC-MS, and the samples were heated at 90 °C for an additional 24 h and analyzed directly via GC-MS.

^b Reactions were flushed with ethylene and stirred under 50 psi in a pressure flask. NR: No reaction.

NMR Studies and Attempted Crystallizations

In parallel with our efforts to screen our bifunctional PyOX precatalyst **1** under different reaction conditions, we attempted to obtain single crystals of various Pd(II) and Pt(II) complexes. Crystallization trials were run via slow diffusion using nitromethane, 1:1 nitromethane/benzene, or acetonitrile as the strong solvent and diethyl ether or pentane as the weak solvent. Unfortunately, our attempts thus far have been unsuccessful. To further probe the dynamics of the PyOX precatalyst with the metal salt, ^1H NMR spectra were obtained in CD_3NO_2 before and after the addition of 1 equivalent of $\text{Pd}(\text{MeCN})_2\text{Cl}_2$ (Figure 2). In the presence of Pd(II), all of the ligand peaks broaden significantly. Furthermore, the organocatalyst alkyl tether peaks have a downfield shift. Broadening of the precatalyst peaks upon addition of $\text{Pd}(\text{MeCN})_2\text{Cl}_2$ is consistent with slow exchange between two or more complexes. The broadening and shifting of the aminoethyl peaks (the 4 methylene protons originally at 2.8 ppm, and the methyl protons at 2.3 ppm, Figure 2, bottom) suggests an undesirable interaction between the metal and the amine, presumably in an intermolecular fashion. A ^1H NMR spectrum of the Boc-protected precatalyst **11** in the presence of $\text{Pd}(\text{MeCN})_2\text{Cl}_2$ was obtained (Figure 3). The ligand peaks remain sharp and downfield shifts are observed for the pyridyl and oxazoline protons after addition of Pd(II) (Figure 3, top), while the aminoethyl and methyl protons at 3.4 and 2.9 ppm are not shifted. The noticeable difference in NMR signals between the carbamate **11** and precatalyst amine **1** upon the addition of Pd(II) is consistent with the amine (but not the carbamate) participating in undesirable intermolecular coordination with the metal, which may also occur under the reaction conditions and preclude substrate binding and activation. To the carbamate **11** and $\text{Pd}(\text{MeCN})_2\text{Cl}_2$ (1 equiv) was added AgBF_4 (1 equiv) as a solution in CD_3NO_2 , and the solution was shaken for 1 hour and filtered through a PTFE syringe filter, before a stock solution of cyclopentene (1 equiv) in CD_3NO_2 was added. Relative to a control sample without catalyst, there were no observed changes in the ^1H NMR for the cyclopentene peaks. This indicated that a Pd–alkene complex did not form to a significant degree, though reactions on transiently-coordinated ligands are possible.

Conclusions

We have undertaken a strategy for the design and prioritization of potential bifunctional catalysts using DFT calculations on putative catalytic intermediates before and after C–C bond formation. This approach was utilized to prioritize a square planar pyridyl-oxazoline metal catalyst with aryl spacer connected to an organocatalytic amine. The novel precatalyst **1** was synthesized and screened with a variety of group 10 metals for the addition of cyclopenta-

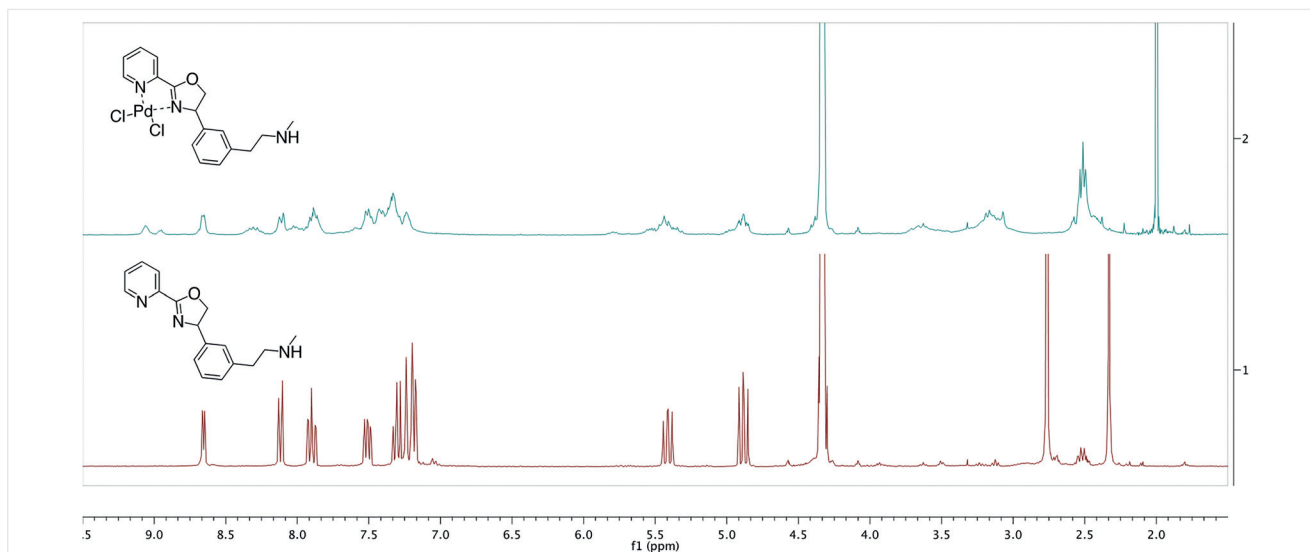


Figure 2 ¹H NMR (CD₃NO₂, 300 MHz) spectra of PyOX precatalyst **1** (bottom) and its Pd(II) complex (top)

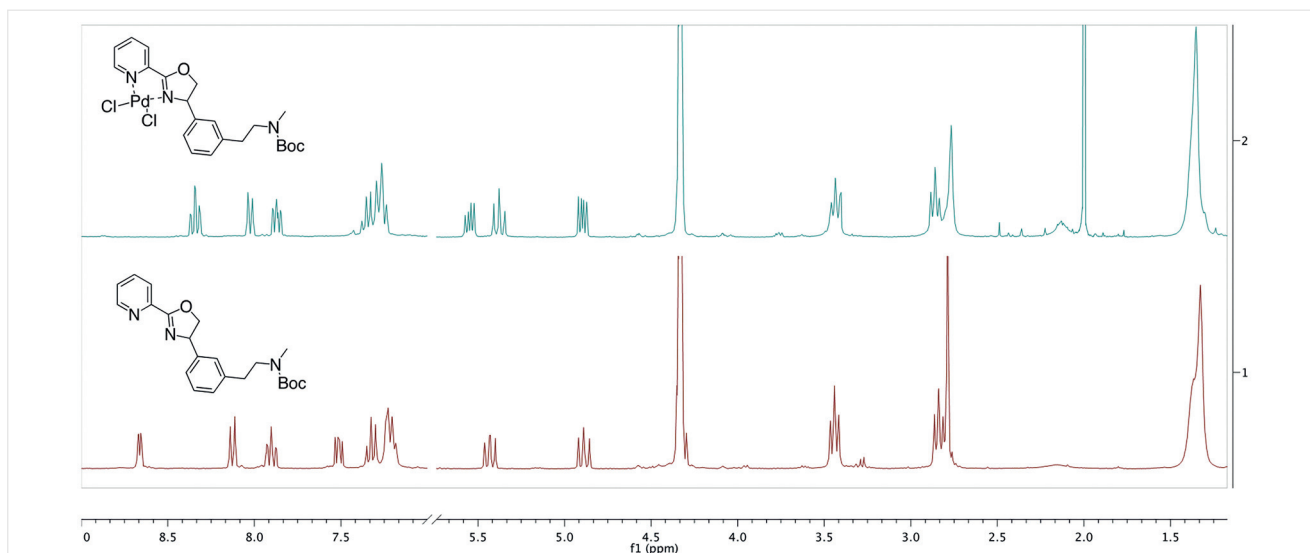


Figure 3 ¹H NMR (CD₃NO₂, 300 MHz) spectra of Boc-protected PyOX precatalyst **11** (bottom) and its Pd(II) complex (top)

none or methyl acetoacetate to alkenes or alkynes. Due to the lack of desired reactivity, suppression of olefin oligomerization, and ¹H NMR data, we conclude there is a lack of a discrete complex between the bifunctional precatalyst and the pi-acid due to intermolecular amine–metal interactions. We hypothesize that analogous tridentate bifunctional ligands may give a discrete catalyst coordination mode more suitable for alkene/alkyne activation, while minimizing catalyst–catalyst interactions. Studies in this area are underway.

All reactions utilized magnetic stirring, unless otherwise noted. All reagents and solvents were purchased from commercial vendors and used as received, except for MeNO₂, which was distilled and stored

over 4 Å mol sieves prior to use. Reactions were performed in ventilated fume hoods with magnetic stirring and oil bath heating, unless otherwise noted. Chilled reactions (below –10 °C) were performed in an acetone bath in a vacuum Dewar, using a Neslab CC 100 immersion cooler. Deionized H₂O was purified by charcoal filtration and used for reaction workups and in reactions with H₂O. NMR spectra were recorded on Varian 300 MHz or 400 MHz spectrometers as indicated. Proton and carbon chemical shifts are reported in parts per million (ppm; δ) relative to TMS, CDCl₃, or CD₃NO₂ (¹H δ = 0, ¹³C δ = 77.16, or ¹H δ = 4.33, respectively). NMR data are reported as follows: chemical shifts, multiplicity (standard abbreviations; and obs: obscured, app: apparent, sxt: sextet, comp: complex overlapping signals); coupling constant(s) in Hz; integration. Unless otherwise indicated, NMR data were collected at 25 °C. NMR data were processed using either MestreNova or ACD/NMR Processor Academic Edition software. Flash chromatography was performed using Biotage SNAP cartridges filled

with 40–60 μm silica gel, or C18 reverse phase columns (Biotage® SNAP Ultra C18 or Isco Redisp® Gold C18Aq) on Biotage Isolera systems, with photodiode array UV detectors. Analytical TLC was performed on Agela Technologies glass plates with 0.25 mm silica gel with F254 indicator. Visualization was accomplished with UV light (254 nm) and aq KMnO_4 stain followed by heating, unless otherwise noted. Tandem liquid chromatography/mass spectrometry (LC-MS) was performed on a Shimadzu LCMS-2020 with autosampler, photodiode array detector, and single-quadrupole MS with ESI and APCI dual ionization, using a Peak Scientific nitrogen generator. Unless otherwise noted, a standard LC-MS method was used to analyze reactions and reaction products: Phenomenex Gemini C18 column (100 \times 4.6 mm, 3 μm particle size, 110 Å pore size); column temperature 40 $^\circ\text{C}$; 5 μL of sample in MeOH or MeCN at a nominal concentration of 1 mg/mL was injected, and peaks were eluted with a gradient of 25–95% MeCN/ H_2O (both with 0.1% formic acid) over 5 min, then 95% MeCN/ H_2O for 2 min. Purity was measured by UV absorbance at 210 or 254 nm. High-resolution mass spectra were obtained at the University of Cincinnati Environmental Analysis Service Center with an Agilent 6540 Accurate-Mass Q-TOF LC/MS with ESI and APCI ionization. Gas chromatography/mass spectrometry (GC-MS) was performed with Agilent Technologies 6850 GC with 5973 MS detector, and Agilent HP-5S or Phenomenex Zebron ZB-5MSi Guardian columns (30 m, 0.25 mm ID, 0.25 μm film thickness). IR spectra were obtained as a thin film on ZnSe plate using a Thermo Scientific Nicolet iS5 spectrophotometer. Chemical names were generated and select chemical properties were calculated using either ChemAxon Marvin suite or ChemDraw Professional 15.1. A VWR® Analogue vortex mixer fitted with a 5 \times 5" sample box with divider was used to shake reactions in glass 1.5 mL HPLC vials. The positive control 2-ethylcyclopentanone was synthesized according to a reported procedure.³⁸ All previously reported and characterized compounds are denoted by their CAS numbers.

DFT Calculations

Starting point geometries for enamine–alkyne complex calculations were set by starting with enamine–Pd(II)–ethylene complex (before C–C bond formation) and adduct (after C–C bond formation) from Table 2, entry 1. These complexes were drawn within the Avogadro molecular visualization program³⁹ and subjected to preliminary optimization with molecular mechanics using the auto-optimization feature (force field set to UFF, 4 steps per update, and steepest descent algorithm). A total of 9 different enamine complexes (due to different dihedral angles around the organocatalyst alkyl tether) and the *E*- and *Z*-iminium adduct isomers were calculated for each precatalyst. Geometries were then optimized and energies were calculated by DFT using the B3PW91 functional and the basis sets LANL2DZ for all metals and cc-pVDZ for other atoms, using the PCM solvation model with dichloromethane. Enthalpies and free energies were calculated at 298.15 K using unscaled harmonic vibrational frequencies. All calculations were performed with Gaussian 09 on the Pèrre cluster at Marquette University.

Synthesis of *cis*-[Pt(DMSO)₂I₂]

This was prepared from a procedure adapted from that reported by Vos.⁴⁰ *cis*-[Pt(DMSO)₂Cl₂] (0.250 g, 0.592 mmol) and KI (0.295 g, 1.78 mmol) were added to an oven-dried 4 mL vial with stir bar, and minimal DMSO (1.5 mL) was added to dissolve the salts. The mixture was heated at 50 $^\circ\text{C}$ for 3 h. After cooling to r.t., the solution was diluted with *i*-PrOH (2 mL), followed by H_2O (10 mL). An orange precipitate

formed, which was collected by vacuum filtration after 30 min, then dried under high vacuum to yield the title compound as an orange solid (0.215 g, 60%).

Synthesis of PyOX Precatalyst

2-(3-Bromophenyl)ethanamine (3)

[CAS Reg. No. 58971-11-2]

This compound was prepared using a procedure described by Leung and co-workers.²⁹ LiAlH_4 (3.04 g, 80.0 mmol) was added to a 250 mL oven-dried round-bottomed flask with stir bar and sealed under N_2 with a septum. Anhyd THF (100 mL) was added, and the flask was cooled to -5°C in an ice/salt bath. Conc H_2SO_4 (3.9 g, 40 mmol) was added dropwise by a syringe, and the resulting mixture was stirred at -5°C for 1 h. A solution of 3-bromobenzenenitrile (9.8 g, 50 mmol) in anhyd THF (5.0 mL) was added dropwise, and the flask was removed from the ice bath when the addition was complete, and the reaction mixture was stirred at r.t. for 1 h. The reaction was then cooled back to -5°C and quenched by the addition of 1:1 THF/ H_2O (12.4 mL). Et_2O (50 mL) was added, followed by aq NaOH (3.6 M, 24.4 mL). The mixture was filtered through Celite, and the solids were washed well with additional Et_2O (6 \times 50 mL). H_2O (100 mL) was added and the phases were separated, and the organic phase was dried (Na_2SO_4), filtered, and concentrated under vacuum to give amine **3** as a yellow oil (8.97 g, 90%).

IR (thin film): 3363, 3284, 2932, 2863, 1656, 1592, 1565, 1472, 1425, 1372, 1323, 775, 690, 664 cm^{-1} .

^1H NMR (300 MHz, CDCl_3): δ = 7.36–7.29 (m, 2 H), 7.20–7.10 (m, 2 H), 2.96 (t, J = 6.9 Hz, 2 H), 2.72 (t, J = 6.9 Hz, 2 H), 1.19 (br s, 2 H).

^{13}C NMR (75 MHz, CDCl_3): δ = 142.3, 131.9, 130.1, 129.4, 127.6, 122.6, 43.4, 39.8.

tert-Butyl *N*-[2-(3-Bromophenyl)ethyl]carbamate (4)

[CAS Reg. No. 153732-25-3]

Amine **3** (8.93 g, 44.6 mmol) was added to a 250 mL oven-dried round-bottomed flask with stir bar and sealed with a septum under N_2 . Anhyd THF (70 mL) and Et_3N (12.4 mL, 89.0 mmol) were added and the reaction mixture was stirred for 15 min at 0 $^\circ\text{C}$ before Boc anhydride (10.72 g, 49.1 mmol) was added. The mixture was warmed to r.t. and stirred for 2 h, then it was diluted with CH_2Cl_2 (100 mL) and H_2O (100 mL). The organic layer was separated and the aqueous layer was extracted with CH_2Cl_2 (3 \times 100 mL). The combined organic extracts were washed with brine (100 mL), dried (Na_2SO_4), filtered, and concentrated under vacuum to afford a yellow oil. The crude material was purified by flash chromatography (340 g SiO_2 column, 0–20% EtOAc/hexanes gradient) to yield **4** as a clear yellow oil (11.0 g, 82%); R_f = 0.70 (50:50 EtOAc/hexanes).

IR (thin film): 3343, 2976, 2931, 1687, 1596, 1567, 1508, 1474, 1426, 1365, 1343, 1269, 1247, 1162, 777, 692, 670 cm^{-1} .

^1H NMR (300 MHz, CDCl_3): δ = 7.37–7.34 (m, 2 H), 7.20–7.10 (m, 2 H), 4.59 (br s, 1 H), 3.36 (q, J = 6.9 Hz, 2 H), 2.77 (t, J = 7.0 Hz, 2 H), 1.44 (s, 9 H).

^{13}C NMR (75 MHz, CDCl_3): δ = 155.9, 141.5, 132.0, 130.2, 129.6, 127.6, 122.7, 79.5, 41.7, 36.0, 28.5.

tert-Butyl *N*-[2-(3-Bromophenyl)ethyl]-*N*-methylcarbamate (5)

[CAS Reg. No. 153732-25-3]

In a 50 mL oven-dried round-bottomed flask, a mixture of carbamate **4** (10.8 g, 35.8 mmol) and powdered KOH (3.01 g, 53.7 mmol) in anhyd DMSO (20 mL) was stirred at r.t. for 5 min. Then MeI (3.34 mL, 53.7 mmol) was slowly added and the reaction mixture was stirred at r.t. for 48 h under N₂. Aq NH₄Cl (25%, 450 mL) was added and the product was extracted with EtOAc (4 × 150 mL). The combined organic layers were washed with brine (100 mL), dried (Na₂SO₄), filtered, and concentrated under vacuum to afford a yellow oil. The crude material was purified by flash chromatography (340 g SiO₂ column, 0–20% EtOAc/hexanes gradient) to yield carbamate **5** as a clear yellow oil (9.8 g, 87%); *R*_f = 0.84 (50:50 EtOAc/hexanes).

IR (thin film): 2974, 2929, 1688, 1596, 1568, 1475, 1424, 1390, 1364, 1214, 1232, 772, 693, 664 cm⁻¹. Note: some peaks are broadened/doubled due to carbamate rotamers.

¹H NMR (300 MHz, CDCl₃): δ = 7.35–7.33 (m, 2 H), 7.18–7.09 (m, 2 H), 3.42 (t, *J* = 6.9 Hz, 2 H), 2.87–2.78 (m, 5 H), 1.44–1.38 (m, 9 H).

¹³C NMR (75 MHz, CDCl₃): δ = 155.6, 141.7, 131.9, 130.1, 129.4, 127.7, 122.5, 79.5, 50.5, 34.3, 33.8, 28.4.

tert-Butyl N-[2-(3-Ethenylphenyl)ethyl]-N-methylcarbamate (6)

A solution of potassium vinyltrifluoroborate (2.10 g, 15.7 mmol), PdCl₂ (53.2 mg, 0.30 mmol), PPh₃ (236 mg, 0.90 mmol), Cs₂CO₃ (14.7 g, 45.0 mmol), and aryl bromide **5** (4.71 g, 15.0 mmol) in THF/H₂O (9:1, 30 mL) was heated at 85 °C under an argon atmosphere in a 15 mL sealed pressure tube. The reaction mixture was stirred at 85 °C for 22 h, then cooled to r.t. and diluted with H₂O (45 mL) followed by extraction with CH₂Cl₂ (3 × 150 mL). The combined organic extracts were washed with brine (50 mL), dried (Na₂SO₄), filtered, and concentrated under vacuum. The crude product was purified by flash chromatography (100 g SiO₂, 0–10% EtOAc/hexanes) to yield **6** as a clear yellow oil (3.51 g, 90%); *R*_f = 0.70 (50:50).

IR (thin film): 2975, 2930, 1690, 1632, 1602, 1582, 1480, 1451, 1422, 1391, 1364, 1163, 1133, 905, 878, 798, 771, 713 cm⁻¹. Note: some peaks are broadened/doubled due to carbamate rotamers.

¹H NMR (300 MHz, CDCl₃): δ = 7.33–7.07 (m, 4 H), 6.69 (dd, *J* = 17.6, 10.9 Hz, 1 H), 5.74 (d, *J* = 17.6 Hz, 1 H), 5.21 (d, *J* = 10.9 Hz, 1 H), 3.42 (t, *J* = 7.0 Hz, 2 H), 2.84–2.79 (m, 5 H), 1.44–1.39 (m, 9 H).

¹³C NMR (75 MHz, CDCl₃): δ = 155.7, 139.6, 137.8, 136.9, 128.7, 128.5, 126.9, 124.3, 113.9, 79.3, 50.9, 35.0, 34.6, 28.4.

HRMS (ESI⁺): *m/z* [M + Na]⁺ calcd for C₁₆H₂₃NO₃Na: 284.1626; found: 284.1621.

tert-Butyl N-Methyl-N-[2-[3-(oxiran-2-yl)phenyl]ethyl]carbamate (7)

In a 25 mL oven-dried round-bottomed flask, a solution of olefin **6** (1.03 g, 3.92 mol) in anhyd CH₂Cl₂ (15 mL) was cooled to 0 °C. While stirring, mCPBA (1.26 g, 5.11 mmol) was slowly added, and the reaction mixture was stirred for 3 h at 0 °C. The mixture was allowed to warm to 20 °C and stirred for an additional 16 h. Then the mixture was diluted with hexanes (200 mL), and the organic layer was washed with 50% sat. aq NaHCO₃ (3 × 50 mL) and brine (50 mL), dried (Na₂SO₄), filtered, and concentrated under vacuum to afford a pale yellow oil. The crude product was purified by flash chromatography (100 g SiO₂, 0–20% EtOAc/hexanes) to yield epoxide **7** as a colorless oil (940 mg, 75%); *R*_f = 0.77 (50:50 EtOAc/hexanes).

IR (thin film): 2975, 2930, 1687, 1480, 1451, 1391, 1364, 1161, 1132, 879, 792, 771, 702 cm⁻¹. Note: some peaks are broadened/doubled due to carbamate rotamers.

¹H NMR (300 MHz, CDCl₃): δ = 7.30–7.25 (m, 1 H), 7.14–7.08 (m, 3 H), 3.84 (dd, *J* = 4.1, 2.6 Hz, 1 H), 3.42 (t, *J* = 7.6 Hz, 2 H), 3.14 (dd, *J* = 5.5, 4.1 Hz, 1 H), 2.83–2.78 (m, 6 H), 1.44–1.39 (m, 9 H).

¹³C NMR (75 MHz, CDCl₃): δ = 155.7, 139.6, 137.8, 136.9, 128.7, 128.5, 126.9, 124.3, 113.9, 79.3, 50.9, 35.0, 34.6, 28.5.

HRMS (ESI⁺): *m/z* [M + Na]⁺ calcd for C₁₆H₂₃NO₃Na: 300.1576; found: 300.1570.

tert-Butyl N-[2-[3-(1-Azido-2-hydroxyethyl)phenyl]ethyl]-N-methylcarbamate (8)

NaN₃ (504 mg, 7.75 mmol) was added to a stirred suspension of epoxide **7** (715 mg, 2.58 mmol) in H₂O (12 mL) in a 25 mL round-bottomed flask. The reaction mixture was heated at 60 °C in an oil bath for 32 h. Then the flask was cooled to r.t., and H₂O (10 mL) was added. The aqueous phase was extracted with EtOAc (3 × 40 mL) and the combined organic extracts were washed with brine (40 mL), dried (Na₂SO₄), and concentrated under vacuum. The crude product was purified by flash chromatography (100 g SiO₂, 0–60% EtOAc/hexanes) to yield azide **8** as a colorless oil (533 mg, 71%); *R*_f = 0.62 (50:50 EtOAc/hexanes).

IR (thin film): 3425, 2976, 2931, 2868, 2096, 1667, 1482, 1451, 1428, 1393, 1365, 1249, 1161, 1134, 876, 792, 771, 706 cm⁻¹. Note: some peaks are broadened/doubled due to carbamate rotamers.

¹H NMR (300 MHz, CDCl₃): δ = 7.32–7.30 (m, 1 H), 7.23–7.12 (m, 3 H), 4.63 (t, *J* = 6.2 Hz, 1 H), 3.75 (m, 2 H), 3.44–3.42 (m, 2 H), 2.83–2.78 (m, 5 H), 2.66–2.51 (br s, 1 H), 1.38 (br s, 9 H).

¹³C NMR (75 MHz, CDCl₃): δ = 155.8, 140.0, 136.8, 129.3, 129.1, 129.0, 127.8, 125.3, 79.5, 67.7, 66.5, 50.8, 50.1, 34.5, 34.0, 28.5.

HRMS (ESI⁺): *m/z* [M + Na]⁺ calcd for C₁₆H₂₄N₄O₃Na: 343.1746; found: 343.1741.

tert-Butyl N-[2-[3-(1-Amino-2-hydroxyethyl)phenyl]ethyl]-N-methylcarbamate (9)

To a 50 mL round-bottomed flask were added azide **8** (503 mg, 1.57 mmol) and MeOH (100 mL). The headspace was flushed with N₂ for 5 min, and Pd/C (167 mg, 0.157 mmol) was added. The flask was sealed and purged with H₂. The reaction mixture was stirred at r.t. for 4 h under a positive pressure of H₂ using a balloon. The mixture was filtered through a Celite plug, and the filtrate was condensed down under vacuum to yield amine **9** as a colorless oil (442 mg, 96%).

IR (thin film): 3355, 3297, 2974, 2929, 2865, 1686, 1481, 1451, 1392, 1364, 1305, 1248, 1215, 1162, 1133, 1049, 877, 823, 794, 771, 706 cm⁻¹. Note: some peaks are broadened/doubled due to carbamate rotamers.

¹H NMR (300 MHz, CDCl₃): δ = 7.30–7.09 (m, 5 H), 4.02 (dd, *J* = 7.9, 4.4 Hz, 1 H), 3.72 (dd, *J* = 10.7, 4.4 Hz, 1 H), 3.55 (dd, *J* = 10.7, 7.9 Hz, 1 H), 3.44–3.41 (m, 2 H), 2.83–2.80 (m, 5 H), 1.38 (s, 9 H).

¹³C NMR (75 MHz, CDCl₃): δ = 155.8, 143.2, 139.6, 128.9, 128.1, 127.2, 124.5, 79.4, 68.2, 57.4, 50.8, 34.6, 34.1, 28.5.

HRMS (ESI⁺): *m/z* [M + H]⁺ calcd for C₁₆H₂₇N₂O₃: 295.2022; found: 295.2016.

tert-Butyl N-[2-[3-(2-Hydroxy-1-[(pyridin-2-yl)formamido]ethyl)phenyl]ethyl]-N-methylcarbamate (10)

To an oven-dried 100 mL round-bottomed flask were added amine **9** (450 mg, 1.53 mmol) and anhyd CH₂Cl₂ (30 mL). Then picolinic acid (190 mg, 1.53 mmol), HOBt (370 mg, 2.29 mmol), EDC-HCl (440 mg, 2.29 mmol), and DIPEA (523 μL, 3.06 mmol) were sequentially added

and the reaction mixture was stirred at r.t. for 16 h under N₂. After 16 h, the mixture was concentrated under reduced pressure and taken up into EtOAc (100 mL) before being washed with H₂O (2 × 30 mL), sat. aq NaHCO₃ (2 × 30 mL), and brine (50 mL). The organic layer was dried (Na₂SO₄), filtered, and concentrated under vacuum. The crude oil was purified by flash chromatography (50 g SiO₂, 0–8% MeOH/CH₂Cl₂) to yield a mixture of amide **10** and an ester by-product formed from additional reaction of the primary alcohol with picolinic acid. This by-product was easily converted back to **10** by redissolving the crude mixture in H₂O/THF (1:3, 32 mL) and adding LiOH·H₂O (25.7 mg, 0.613 mmol), then stirring at r.t. for 30 min. The aqueous layer was extracted with CH₂Cl₂ (4 × 20 mL), and the combined organic layers were dried (Na₂SO₄), filtered, and concentrated under vacuum to yield exclusively amide **10** as a pale yellow oil (432 mg, 71% over 2 steps); *R*_f = 0.78 (90:10 CH₂Cl₂/MeOH).

IR (thin film): 3385, 2974, 2930, 1665, 1591, 1570, 1516, 1484, 1465, 1433, 1393, 1365, 1164, 1135 cm⁻¹. Note: some peaks are broadened/doubled due to carbamate rotamers.

¹H NMR (300 MHz, CDCl₃): δ = 8.77 (br s, 1 H), 8.57 (d, *J* = 4.7 Hz, 1 H), 8.19 (dd, *J* = 7.8, 0.8 Hz, 1 H), 7.85 (t, *J* = 7.8 Hz, 1 H), 7.44 (dd, *J* = 7.6, 4.8 Hz, 1 H), 7.30–7.04 (m, 5 H), 5.22 (dt, *J* = 7.6, 4.8 Hz, 1 H), 3.99 (t, *J* = 4.8 Hz, 2 H), 3.41–3.39 (m, 2 H), 2.84–2.81 (m, 7 H), 1.38–1.34 (m, 9 H).

¹³C NMR (75 MHz, CDCl₃): δ = 164.7, 149.8, 148.3, 139.7, 139.5, 137.5, 129.2, 128.9, 128.6, 127.5, 126.4, 125.0, 122.5, 79.5, 66.8, 56.1, 50.8, 49.9, 34.5, 28.5.

HRMS (ESI⁺): *m/z* [M + H]⁺ calcd for C₂₂H₃₀N₃O₄: 400.2236; found: 400.2231.

tert-Butyl N-methyl-N-(2-{3-[2-(pyridin-2-yl)-4,5-dihydro-1,3-oxazol-4-yl]phenyl}ethyl)carbamate (11**)**

In an oven-dried 50 mL round-bottomed flask, a solution of amide **10** (413 mg, 1.03 mmol) in anhyd CH₂Cl₂ (15 mL) was cooled to –20 °C under N₂. Deoxo-Fluor® (226 μL, 1.23 mmol) was added dropwise, and the mixture was stirred at –20 °C for 1 h under N₂. After 1 h, the reaction mixture was allowed to warm up to r.t. and the mixture was stirred for an additional 1 h. The reaction was quenched with sat. aq NaHCO₃ (10 mL) and H₂O (10 mL), and the aqueous layer was extracted with CH₂Cl₂ (3 × 10 mL). The combined organic layers were washed with brine (20 mL), dried (Na₂SO₄), filtered, and concentrated under vacuum. The crude oil was purified by flash chromatography (25 g SiO₂, 0–6% MeOH/CH₂Cl₂) to afford oxazoline **11** as an orange oil (346 mg, 88%); *R*_f = 0.62 (90:10 CH₂Cl₂/MeOH).

IR (thin film): 2974, 2929, 1687, 1640, 1477, 1441, 1391, 1363, 1308, 1248, 1164, 1134, 1099, 1043, 964, 878, 799, 772, 744, 706 cm⁻¹. Note: some peaks are broadened/doubled due to carbamate rotamers.

¹H NMR (400 MHz, CDCl₃): δ = 8.76–8.74 (m, 1 H), 8.17 (d, *J* = 7.9 Hz, 1 H), 7.81 (td, *J* = 7.9, 1.7 Hz, 1 H), 7.44 (ddd, *J* = 7.4, 5.0 Hz, 1.0 Hz, 1 H), 7.31–7.29 (m, 1 H), 7.19–7.10 (m, 3 H), 5.44 (dd, *J* = 10.1, 8.7 Hz, 1 H), 4.90 (dd, *J* = 10.1, 8.7 Hz, 1 H), 4.38 (t, *J* = 8.7 Hz, 1 H), 3.41 (m, 2 H), 2.9–2.7 (comp, 5 H), 1.43–1.39 (br s, 9 H).

¹³C NMR (75 MHz, CDCl₃): δ = 164.0, 155.7, 149.9, 146.8, 142.1, 140.0, 136.8, 129.1, 128.4, 127.4, 125.9, 124.9, 124.4, 79.4, 75.4, 70.4, 51.0, 34.7, 34.2, 28.5.

HRMS (ESI⁺): *m/z* [M + H]⁺ calcd for C₂₂H₂₈N₃O₃: 382.2131; found: 382.2125.

Methyl(2-{3-[2-(pyridin-2-yl)-4,5-dihydro-1,3-oxazol-4-yl]phenyl}ethyl)amine (1**)**

To a solution of carbamate **11** (157 mg, 0.142 mmol) in anhyd CH₂Cl₂ (15.0 mL) in a 50 mL round-bottomed flask was added TFA (15.0 mL, 20.6 mmol) dropwise. The reaction mixture was stirred for 10 min at 20 °C. After 10 min, the mixture was added dropwise into sat. aq NaHCO₃ (400 mL). The aqueous layer was extracted with CH₂Cl₂/MeOH (9:1; 5 × 100 mL). The combined organic layers were dried (Na₂SO₄), filtered, and concentrated under vacuum. The crude oil was purified by flash chromatography (12 g C18 cartridge, 0–80% 0.5 N NH₃ in MeOH/H₂O) to afford amine **1** as a colorless oil (64 mg, 55%); *R*_f = 0.04 (90:10 CH₂Cl₂/MeOH).

IR (thin film): 3394, 3056, 2934, 2801, 1640, 1583, 1570, 1471, 1441, 1362, 1248, 1102, 1043, 958, 801, 745, 706 cm⁻¹.

¹H NMR (300 MHz, CDCl₃): δ = 8.75 (d, *J* = 4.8 Hz, 1 H), 8.18 (d, *J* = 7.9 Hz, 1 H), 7.81 (t, *J* = 7.9 Hz, 1 H), 7.46–7.42 (m, 1 H), 7.32–7.27 (m, 1 H), 7.19–7.14 (comp, 3 H), 5.44 (dd, *J* = 10.1, 8.7 Hz, 1 H), 4.90 (dd, *J* = 10.1, 8.7 Hz, 1 H), 4.44 (app t, *J* = 8.7 Hz, 1 H), 2.84–2.80 (comp, 4 H), 2.42 (s, 3 H), 1.11 (br s, 1 H).

¹³C NMR (75 MHz, CDCl₃): δ = 163.9, 149.9, 146.8, 142.1, 140.8, 136.8, 129.0, 128.2, 127.3, 125.9, 124.8, 124.4, 75.4, 70.4, 53.3, 36.5, 36.6.

HRMS (ESI⁺): *m/z* [M + H]⁺ calcd for C₁₇H₂₀N₃O: 282.1606; found: 282.1601.

Funding Information

American Chemical Society Petroleum Research Fund (55732-DN11)

Acknowledgment

We thank Dr. Sheng Cai for assistance with LC-MS and NMR instruments, Profs. James Gardinier and Chae Yi for helpful comments, Marquette University for startup funding, and the American Chemical Society Petroleum Research Fund (grant number 55732-DN11) for support of this project. We also thank ChemAxon and ACD/Labs for use of their NMR prediction and processing software. **Author Contributions:** Designed catalysts: C.D., E.G.; Performed DFT calculations: E.G.; Synthesized and characterized precatalysts: E.G.; Screened reactions: E.G., J.D.P.; Performed NMR studies: E.G.; Performed crystallization studies: E.G.; Wrote the manuscript: C.D., E.G.

Supporting Information

Supporting information for this article is available online at <https://doi.org/10.1055/s-0037-1610285>. Included are ¹H and ¹³C NMR spectra, representative Gaussian input files, and Cartesian coordinates for select DFT-optimized structures; Figure S1: DFT optimized cis/trans ethylene coordination for precatalyst **1**; Figure S2: DFT optimized Cu(I) intermediates for Table 2, entry 12; Figure S3: Conformational sampling of DFT optimized **1**-complex; Table S1: Complete set of DFT calculations for C–C bond formation with variable tether lengths and positions, with both Pd and Pt; Table S2: DFT calculations for intramolecular coordination of amine to metal center for various tether lengths and positions; Table S3: DFT calculations of structures with fixed distances between enamine and ethylene.

References

- (1) McCartney, D.; Guiry, P. J. *Chem. Soc. Rev.* **2011**, *40*, 5122.
- (2) Xu, S.; Negishi, E.-I. *Acc. Chem. Res.* **2016**, *49*, 2158.
- (3) Hack, D.; Blumel, M.; Chauhan, P.; Philipps, A. R.; Enders, D. *Chem. Soc. Rev.* **2015**, *44*, 6059.
- (4) Binder, J. T.; Crone, B.; Haug, T. T.; Menz, H.; Kirsch, S. F. *Org. Lett.* **2008**, *10*, 1025.
- (5) Yang, T.; Ferrali, A.; Campbell, L.; Dixon, D. J. *Chem. Commun.* **2008**, 2923.
- (6) Jensen, K. L.; Franke, P. T.; Arróniz, C.; Kobbelgaard, S.; Jørgensen, K. A. *Chem. Eur. J.* **2010**, *16*, 1750.
- (7) Xiao, Y.-P.; Liu, X.-Y.; Che, C.-M. *Angew. Chem. Int. Ed.* **2011**, *50*, 4937.
- (8) Montagnac, B.; Vitale, M. R.; Michelet, V.; Ratovelomanana-Vidal, V. *Org. Lett.* **2010**, *12*, 2582.
- (9) Montagnac, B.; Vitale, M. R.; Ratovelomanana-Vidal, V.; Michelet, V. *J. Org. Chem.* **2010**, *75*, 8322.
- (10) Montagnac, B.; Vitale, M. R.; Ratovelomanana-Vidal, V.; Michelet, V. *Eur. J. Org. Chem.* **2011**, 3723.
- (11) Montagnac, B.; Praveen, C.; Vitale, M. R.; Michelet, V.; Ratovelomanana-Vidal, V. *Chem. Commun.* **2012**, *48*, 6559.
- (12) Wang, X.; Widenhoefer, R. A. *Chem. Commun.* **2004**, 660.
- (13) Cucciolito, M. E.; D'Amora, A.; Vitagliano, A. *Organometallics* **2010**, *29*, 5878.
- (14) Geier, M. J.; Gagné, M. R. *J. Am. Chem. Soc.* **2014**, *136*, 3032.
- (15) Nguyen, H.; Gagné, M. R. *ACS Catal.* **2014**, *4*, 855.
- (16) Walsh, P. J.; Kozlowski, M. C. *Fundamentals of Asymmetric Catalysis* (USA), 2009.
- (17) Mo, F.; Dong, G. *Science* **2014**, *345* (6192), 68.
- (18) Mo, F.; Lim, H. N.; Dong, G. *J. Am. Chem. Soc.* **2015**, *137*, 15518.
- (19) Jira, R. *Angew. Chem. Int. Ed.* **2009**, *48*, 9034.
- (20) McDonald, R. I.; Liu, G.; Stahl, S. S. *Chem. Rev.* **2011**, *111*, 2981.
- (21) Sigman, M. S.; Werner, E. W. *Acc. Chem. Res.* **2012**, *45*, 874.
- (22) Melchiorre, P.; Marigo, M.; Carlone, A.; Bartoli, G. *Angew. Chem. Int. Ed.* **2008**, *47*, 6138.
- (23) Fürstner, A. *Acc. Chem. Res.* **2014**, *47*, 925.
- (24) Porter, J. D.; Greve, E.; Alsafran, A.; Benoit, A. R.; Lindeman, S. V.; Dockendorff, C. *Tetrahedron* **2018**, *74*, 4823; *ChemRxiv* **2018**, <https://doi.org/10.26434/chemrxiv.6163430.v1>.
- (25) Stephan, D. W. *Science* **2016**, *354* (6317), aaf7229.
- (26) Hay, P. J.; Wadt, W. R. *J. Chem. Phys.* **1985**, *82*, 270.
- (27) Kendall, R. A.; Dunning, T. H. Jr.; Harrison, R. J. *J. Chem. Phys.* **1992**, *96*, 6796.
- (28) Yoon, N. M.; Brown, H. C. *J. Am. Chem. Soc.* **1968**, *90*, 2927.
- (29) Leung, C.; Tomaszewski, M. J.; Woo, S. PCT Int. Appl. WO 04 60882, **2004**; *Chem. Abstr.* **2004**, *141*, 140172.
- (30) Molander, G. A.; Brown, A. R. *J. Org. Chem.* **2006**, *71*, 9681.
- (31) Wang, H.-Y.; Huang, K.; De Jesús, M.; Espinosa, S.; Piñero-Santiago, L. E.; Barnes, C. L.; Ortiz-Marciales, M. *Tetrahedron: Asymmetry* **2016**, *27*, 91.
- (32) Lal, G. S.; Pez, G. P.; Pesaresi, R. J.; Prozonic, F. M.; Cheng, H. *J. Org. Chem.* **1999**, *64*, 7048.
- (33) Phillips, A. J.; Uto, Y.; Wipf, P.; Reno, M. J.; Williams, D. R. *Org. Lett.* **2000**, *2*, 1165.
- (34) Stork, G.; Brizzolara, A.; Landesman, H.; Szmuszkowicz, J.; Terrell, R. *J. Am. Chem. Soc.* **1963**, *85*, 207.
- (35) de Renzi, A.; Panunzi, A.; Vitagliano, A.; Paiaro, G. *J. Chem. Soc., Chem. Commun.* **1976**, 47.
- (36) Sen, A.; Lai, T.-W. *J. Am. Chem. Soc.* **1981**, *103*, 4627.
- (37) Albietz, P. J.; Yang, K.; Lachicotte, R. J.; Eisenberg, R. *Organometallics* **2000**, *19*, 3543.
- (38) Delort, E.; Velluz, A.; Frérot, E.; Rubin, M.; Jaquier, A.; Linder, S.; Eidman, K. F.; MacDougall, B. S. *J. Agric. Food Chem.* **2011**, *59*, 11752.
- (39) Hanwell, M. D.; Curtis, D. E.; Lonie, D. C.; Vandermeersch, T.; Zurek, E.; Hutchison, G. R. *J. Cheminform.* **2012**, *4*, 17.
- (40) Kowacs, T.; O'Reilly, L.; Pan, Q.; Huijser, A.; Lang, P.; Rau, S.; Browne, W. R.; Pryce, M. T.; Vos, J. G. *Inorg. Chem.* **2016**, *55*, 2685.